coatings

MDPI

Article

Laser Control of Specular and Diffuse Reflectance of Thin Aluminum Film-Isolator-Metal Structures for Anti-Counterfeiting and Plasmonic Color Applications

Michał P. Nowak [1], Bogusz Stępak [2], Mateusz Pielach [3], Yuriy Stepanenko [3], Tomasz Wojciechowski [4], Bartosz Bartosewicz [1], Urszula Chodorow [5], Marcin Jakubaszek [1], Przemysław Wachulak [1] and Piotr Nyga [1,*]

1 Institute of Optoelectronics, Military University of Technology, ul. Kaliskiego 2, 00-908 Warsaw, Poland; michal.nowak@wat.edu.pl (M.P.N.); bartosz.bartosewicz@wat.edu.pl (B.B.); marcin.jakubaszek@wat.edu.pl (M.J.); przemyslaw.wachulak@wat.edu.pl (P.W.)
2 Fluence Sp. z o.o., ul. Kolejowa 5/7, 01-217 Warsaw, Poland; bstepak@fluence.technology
3 Institute of Physical Chemistry, Polish Academy of Sciences, ul. Kasprzaka 44/52, 01-224 Warsaw, Poland; mgpielach@ichf.edu.pl (M.P.); ystepanenko@ichf.edu.pl (Y.S.)
4 International Research Centre MagTop, Institute of Physics, Polish Academy of Sciences, Al. Lotników 32/46, 02-668 Warsaw, Poland; twojcie@ifpan.edu.pl
5 Institute of Applied Physics, Faculty of New Technologies and Chemistry, Military University of Technology, ul. Kaliskiego 2, 00-908 Warsaw, Poland; urszula.chodorow@wat.edu.pl
* Correspondence: piotr.nyga@wat.edu.pl

Abstract: Plasmonic structural color originates from the scattering and absorption of visible light by metallic nanostructures. Stacks consisting of thin, disordered semicontinuous metal films are attractive plasmonic color media, as they can be mass-produced using industry-proven physical vapor deposition techniques. These films are comprised of random nano-island structures of various sizes and shapes resonating at different wavelengths. When irradiated with short-pulse lasers, the nanostructures are locally restructured, and their optical response is altered in a spectrally selective manner. Therefore, various colors are obtained. We demonstrate the generation of structural plasmonic colors through femtosecond laser modification of a thin aluminum film–isolator–metal mirror (TAFIM) structure. Laser-induced structuring of TAFIM's top aluminum film significantly alters the sample's specular and diffuse reflectance depending on the fluence value and the number of times a region is scanned. A "negative image" effect is possible, where a dark field observation mode image is a negative of a bright field mode image. This effect is visible using an optical microscope, the naked eye, and a digital camera. The use of self-passivating aluminum results in a long-lasting, non-fading coloration effect. The reported technique could be used in anti-counterfeiting and security applications, as well as in plasmonic color printing and macroscopic and microscopic marking for personalized fine arts and aesthetic products such as jewelry.

Keywords: plasmon resonance; plasmonic color; aluminum film; femtosecond laser modification; anti-counterfeiting; diffuse reflectance; metal–isolator–metal

Citation: Nowak, M.P.; Stępak, B.; Pielach, M.; Stepanenko, Y.; Wojciechowski, T.; Bartosewicz, B.; Chodorow, U.; Jakubaszek, M.; Wachulak, P.; Nyga, P. Laser Control of Specular and Diffuse Reflectance of Thin Aluminum Film-Isolator-Metal Structures for Anti-Counterfeiting and Plasmonic Color Applications. *Coatings* **2024**, *14*, 1298. https://doi.org/10.3390/coatings14101298

Academic Editor: Angela De Bonis

Received: 17 September 2024
Revised: 7 October 2024
Accepted: 9 October 2024
Published: 11 October 2024

1. Introduction

Colors of the surrounding world originate from dyes and pigments, which absorb part of the visible spectrum and thus modify the reflected light reaching the eyes of the observer. In contrast, structural color originates from a spectrally selective light scattering from micro- and nanostructured surfaces made from often nonabsorbing materials [1]. The vibrant colors of butterflies [2] or beetles [3] are beautiful examples of structural color in nature. Recently, with advances in micro and nanofabrication techniques, there has been increased interest in color generated by engineered dielectric and metallic structures, such as metastructures [4–17] and photonic crystals [18], thin film coatings [19–28], and

metal–dielectric composites [29,30]. Most of the above-referred articles discuss the use of plasmonic structural color, where the color is a function of dimensions and arrangement of plasmonic nanostructures and dielectric counterparts. Several review articles present a wide span of fabrication techniques and applications of plasmonic structural color [31–33].

Plasmonic structural color is considered for fine and applied visual arts [7,22–24,27] and security and anti-counterfeiting [11,29,30], as structures can be designed to exhibit different colors dependent on light polarization [8,11,17,26,27,34–36] and angle of incidence (AOI) [27,37]. Image multiplexing has been demonstrated using polarization, wavelength, mode of observation in transmittance, reflectance [29,30], luminescence [38–40], and upconversion [41].

Especially plasmonic structural color using thin, disordered random metal films is attractive, as they can be mass-produced using industry-proven, scalable physical vapor deposition (PVD) processes [21,22,42–46]. Such structures are natively disordered and random nano-island-type films composed of nanoparticles of various sizes and shapes that resonate at different wavelengths. Thus, they often absorb in a broad spectral range. When exposed to laser radiation, the nanoparticles can be locally modified. Highly spatially localized restructuring originates from light absorption in hotspots [43,44,47], regions of a high local electric field that form when the film is illuminated with light [48]. Thus, the optical response of the film can be altered, and hence, locally, a different color is obtained. Recently, gold and silver thin semicontinuous films deposited on dielectric substrates [45] and placed on top of a metallic mirror with a thin isolator spacer (utilizing gap plasmon modes [49,50]) [12,21,22,25,26], and Fabry–Perot-type structures [27,51,52] have been studied for laser-induced plasmonic structural color printing, and beautiful, polarization-sensitive colors. Studies have also been conducted on the laser coloration of bulk gold and silver samples [53,54]. However, gold is relatively expensive and has an interband transition in the visible spectral range. Therefore, it allows for a limited range of colors. Silver nanostructures, on the other hand, can be chemically unstable and often require a protective layer to achieve long-term stability [22,25]. Thus, aluminum could be an alternative to other plasmonic metals [55], especially for mass-production type applications, due to its low price, CMOS compatibility [56], and self-passivation of the surface [24,57,58]. Aluminum has been extensively used for ordered, lithography-defined structures and metasurface-based plasmonic color [9,10,13–15,17,56,59,60] and also in diffraction control [12]. However, there is limited research on the use of thin, disordered, semicontinuous aluminum films in this area. In our previous study, we investigated laser modification of aluminum-based structures for plasmonic color applications [23].

In this work, we demonstrate femtosecond laser control of color and diffuse reflectance of a thin aluminum film–isolator–metal mirror (TAFIM) structure fabricated using an electron-beam PVD technique. The structure consists of a thin aluminum film deposited on an aluminum mirror coated with a few tens of nanometers thick titanium dioxide (TiO_2) layer. The initial structure is highly reflective and has a gold mirror-like color. Herein, the effects of laser fluence and the dependence of the number of scans on the final color and diffuse reflectance are explored in detail. We report that, for a specific set of laser modification parameters, it is possible to decrease the specular reflectance in the visible spectral range, which results in the "darkening" of the sample when observed in the bright field mode. At the same time, the diffuse reflectance component increases from nearly zero to a few percent, which results in a high signal observed in the dark field mode. This results in a "negative image" effect between the bright and dark field observation modes. Printed images have been stable in both bright and dark field modes for at least 28 months. Our findings could help to realize economically viable laser marking technology and environmentally stable aluminum-based structures for anti-counterfeiting, information encryption, hidden marking, and plasmonic color applications. Furthermore, compared to the state-of-the-art, we present a broader range of colors and stability studies over a much longer time.

2. Materials and Methods

2.1. Fabrication

The TAFIM structure (see Figure 1a) consists of a top thin aluminum film, a TiO_2 spacer, and an aluminum mirror deposited on a glass substrate. The glass substrate was cleaned with ethanol and dried with nitrogen gas shortly before being loaded into a vacuum chamber. The sample was fabricated using an electron beam PVD system (Syrus III 1100, Bühler Leybold Optics, Alzenau, Germany) on substrates at near room temperature. All layers were deposited in a single process without breaking the vacuum. The base pressure of the deposition system was lower than 3×10^{-6} mbar. The aluminum mirror was deposited at a 0.4 nm s^{-1} rate. The top aluminum layer was deposited at a 0.04 nm s^{-1} rate. The titanium dioxide spacer was deposited at a 0.18 nm s^{-1} rate. During the deposition of TiO_2, oxygen gas was supplied to maintain pressure at 2×10^{-4} mbar to ensure proper oxidation of the deposited film. Layer thickness and deposition rates were monitored with a quartz crystal microbalance.

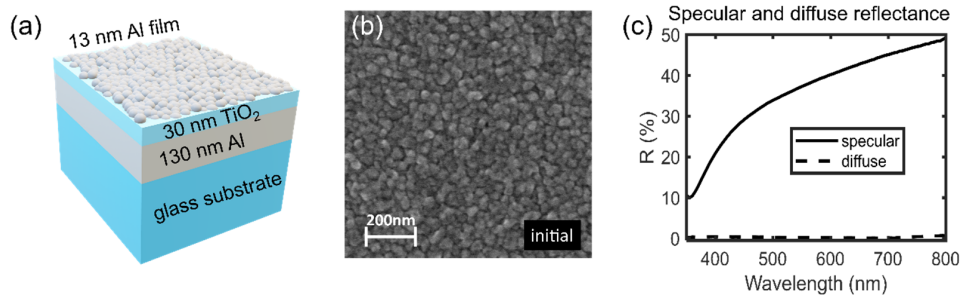

Figure 1. Characteristics of the fabricated TAFIM sample. (**a**) Sketch of a structure of the TAFIM sample. The three-layer stack, deposited on a 1 mm glass substrate, consists of, from the top, a 13 nm thick aluminum film, a 30 nm thick TiO_2 spacer, and a 130 nm thick aluminum mirror. The thickness of the glass substrate is off the scale. (**b**) SEM image of the top Al film. (**c**) Specular and diffuse reflectance of the sample.

2.2. Laser Modification

Laser modification was performed using a linearly polarized, 1030 nm, 300 fs fiber laser (Jasper 20, Fluence Sp. z o.o., Warsaw, Poland). The laser beam was applied to the workpiece through a galvanometric scanner (intelliSCAN 10, Scanlab GmbH, Puchheim, Germany). The beam diameter at $1/e^2$ was 60 µm. The laser fluence was adjusted by a built-in acousto-optic modulator. We used 0.3 m s^{-1} scan speed and 300 kHz pulse repetition rate, which resulted in a distance of 1 µm between the centers of consecutive pulses. To uniformly modify extended areas, we used a raster scan mode, and the distance between lines was equal to 2 µm. The angle between the scanning direction and the polarization axis was set to 25°. The chosen scanning parameters result in a writing speed of 0.36 cm^2 min.

2.3. Characterization

The total and diffuse reflectance of the fabricated and laser-modified structures were measured in the 350–800 nm wavelength range using a UV–VIS spectrophotometer (PerkinElmer, Waltham, MA, USA, Lambda 650) with an integrating sphere (150 mm) module (8° AOI) and unpolarized light. Spectralon was used as a reference sample for reflectance measurements. Specular reflectance was calculated as the difference between total and diffuse reflectance. Additionally, to obtain sample absorption at the laser wavelength (1030 nm), the specular reflectance of the fabricated sample was measured in the 350–1100 nm wavelength range using an Agilent Carry7000 spectrometer (Agilent, Santa Clara, CA, USA) equipped with Universal Measurement Accessory (6° AOI). The morphology of initial and laser-modified samples was examined with a scanning electron microscope (SEM, Auriga, Carl Zeiss, Jena, Germany). We collected cross-sectional SEM images to verify the layer thickness of test samples. We used an optical microscope (Nikon,

Hongkong, China, Eclipse LV150, Nikon T Plan 2.5×/0.075 ∞/0 EPI objective lens) and a digital camera (Nikon, DS-Fi1) to capture printed images in bright and dark field modes. The picture stitching process was performed to acquire images of extended areas. Optical parameters (refractive index, extinction coefficient) and thickness of titanium dioxide and aluminum test samples were determined using a variable angle spectroscopic ellipsometer (Sentech, Berlin, Germany, SE850). To fit the measured data, we used Drude and Tauc–Lorentz models for aluminum and TiO_2, respectively.

2.4. Electromagnetic Simulations and Color Coordinates Calculation

The specular reflectance spectra of the unmodified TAFIM sample were simulated using the Transfer Matrix Method [61], employing the refractive index of aluminum and titanium dioxide retrieved from ellipsometric measurements. For direct comparison with the measurement data, we calculated the reflectance for a 6° AOI. We used a home-written MATLAB script to calculate the CIE 1931 Chromaticity Diagram color coordinates from reflectance spectra assuming spectrally uniform illumination [6,62].

3. Results and Discussion

3.1. Laser Printing

The TAFIM structure (see Figure 1a for a sketch) consists of a three-layer stack comprising, from the top, a 13 nm thick aluminum film, a 30 nm thick TiO_2 spacer, and a 130 nm thick aluminum mirror. All layers were deposited in a single process (see Section 2.1 for details). The top thin aluminum film has a form of densely packed semicontinuous layer (see the SEM image in Figure 1b). Specular and diffuse reflectances (measured for an 8° AOI) of the as-fabricated TAFIM structure are presented in Figure 1c (solid and dashed lines, respectively).

When observed with the naked eye, the TAFIM sample has a high specular reflectance and a gold mirror-like color. However, the color could be adjusted by dielectric spacer thickness, refractive index, and top metallic film thickness [25,51,52]. Supplementary Material Figure S1 presents simulation results of specular reflectance and attainable colors when the TiO_2 spacer layer varies from 30 nm (sample reported in this study) to 100 nm. Due to substantial specular reflectance throughout the visible range, the fabricated TAFIM sample appears bright when observed under an optical microscope in a bright field mode (unmodified regions in the bottom part of Figure 2a). The sample has low diffuse reflectance and thus appears dark/black when observed in dark field mode (unmodified regions in the bottom part of Figure 2b), as in this observation mode, only the scattered light is collected, and the non-scattered beam is blocked from the detector.

The TAFIM sample has about 33% absorptance at the 1030 nm wavelength of the femtosecond laser used for modification (absorptance calculated as 100% minus total reflectance, as the sample has no transmittance due to the thick aluminum mirror). A comparison of measured and simulated specular reflectances, both at a 6° AOI, is presented in Supplementary Material Figure S2.

To test the possibility of laser-induced plasmonic color printing, we investigated how laser fluence impacts the visual appearance of the TAFIM sample, both in specular and diffuse reflectance. We also tested the dependence on the number of times the sample was scanned (overscans) with the laser beam of constant fluence. We modified the TAFIM sample using the femtosecond laser with fluence in the range of about 1–50 mJ cm^{-2} and the number of times a region was scanned (1 to 100 times). Pictures in bright and dark field acquisition mode (collected using an optical microscope; see Section 2.3 for details) of a matrix of squares modified with different laser scanning parameters are presented in Figure 2a,b, respectively. The visual appearance of the TAFIM sample changes significantly due to the laser modification. As fluence or the number of scans increases, the initial darkening of the sample in the bright field mode appears. In contrast, the sample observed in the dark field mode "lights up" and becomes blueish. Sample damage, layers peeling off, is visible in the top right corner of the matrix of squares for the 48 mJ cm^{-2} and the number

of scans of 20 and above. The top aluminum layer modified by laser pulses is present up to a fluence of 37 mJ cm^{-2} and the maximum tested number of overscans (100), as revealed by SEM (Figure 2c and Supplementary Material Figure S4).

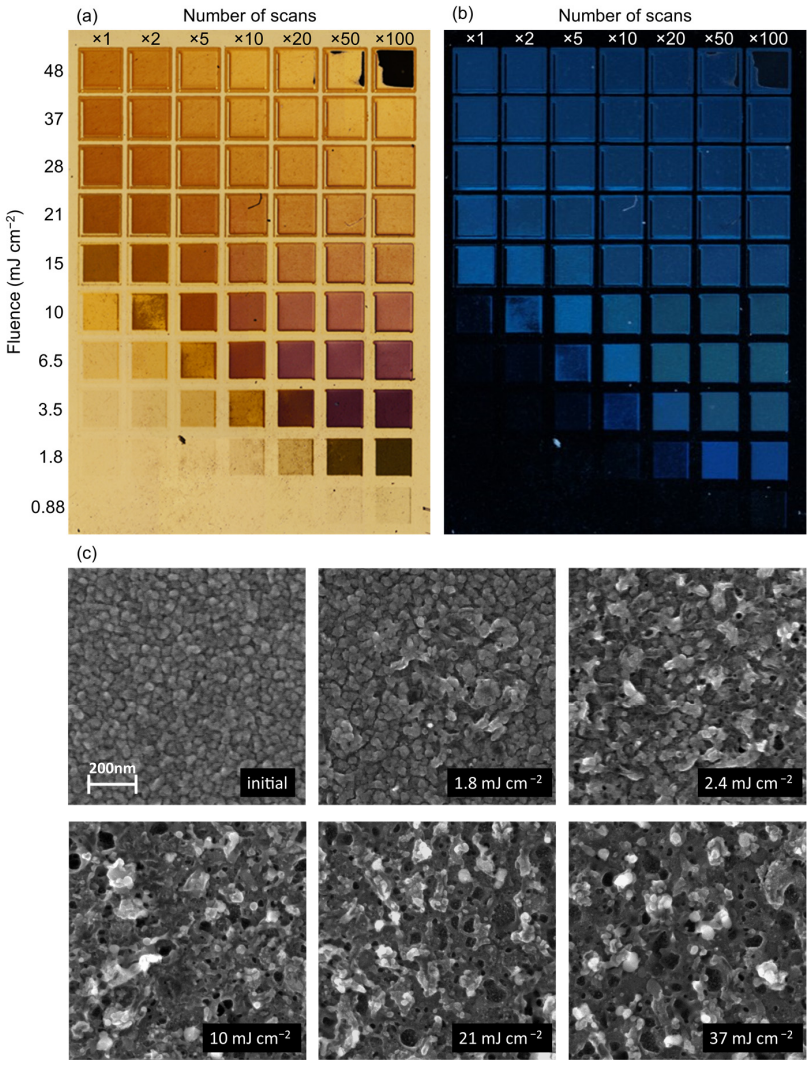

Figure 2. Optical appearance and top Al film nanostructure of fabricated and laser-modified TAFIM structure. (**a**,**b**) Photos taken with an optical microscope of a matrix of squares modified with different laser fluence (vertical direction) and the number of scans repeated on the same area (horizontal direction). Acquisition (**a**) in bright and (**b**) dark field mode. (**c**) SEM images of selected areas of the TAFIM sample before modification (initial; the same image as in Figure 1b) and after raster scanning 20 times with femtosecond laser beam (with fluences: 1.8, 2.4, 10, 21, and 37 mJ cm^{-2}).

The lower-level modification threshold, defined as the fluence for which the alteration of the appearance of the sample becomes visible, is on the order of 1 mJ cm^{-2}. However, tens of scans are necessary to notice changes with the naked eye (see the two bottom rows of squares in Figure 2a,b). Changes in the appearance of the sample in the three bottom rows, corresponding to the lowest fluence range, demonstrate that the low fluence modification results from the accumulation of slight changes in each scan. For laser marking applications, an easy-to-apply approach would be to change one parameter of the scanning setup, e.g., laser fluence. However, Figure 2 shows that high contrast changes can also be achieved by varying only the number of scans. Exploration of space of two parameters, namely the fluence and the number of times a region is scanned with the laser beam, grants a much broader range of colors.

To better illustrate the types of changes induced by laser modification of the TAFIM sample in Figure 3a,b, we present spectral characteristics of specular and diffuse reflectance of unmodified (solid black line, label "initial") and modified regions scanned 20 times with different fluences. Specular and diffuse reflectance spectral characteristics for a fixed fluence of 1.8 mJ cm^{-2} and various scans are presented in Supplementary Material Figure S3. The specular reflectance decreases as the laser fluence increases to 3.5 mJ cm^{-2}. However, with a further increase of fluence, the specular reflectance increases, especially in the red part of the spectrum, and the sample becomes progressively yellowish. The unmodified sample has almost no diffuse reflectance, and laser modification increases it. For the fluence of 3.5–10 mJ cm^{-2}, maximum diffuse reflectance is achieved with a spectral peak greater than 8% located at 500–550 nm. Further increase of laser fluence decreases the diffuse reflectance and shifts the peak to shorter wavelengths. The dependence of the spectral shape of the diffuse reflectance of the modified regions of the TAFIM sample resembles the corresponding absorptance, which could be estimated as inverted specular reflectance (or rigorously calculated as 100% minus the total reflectance).

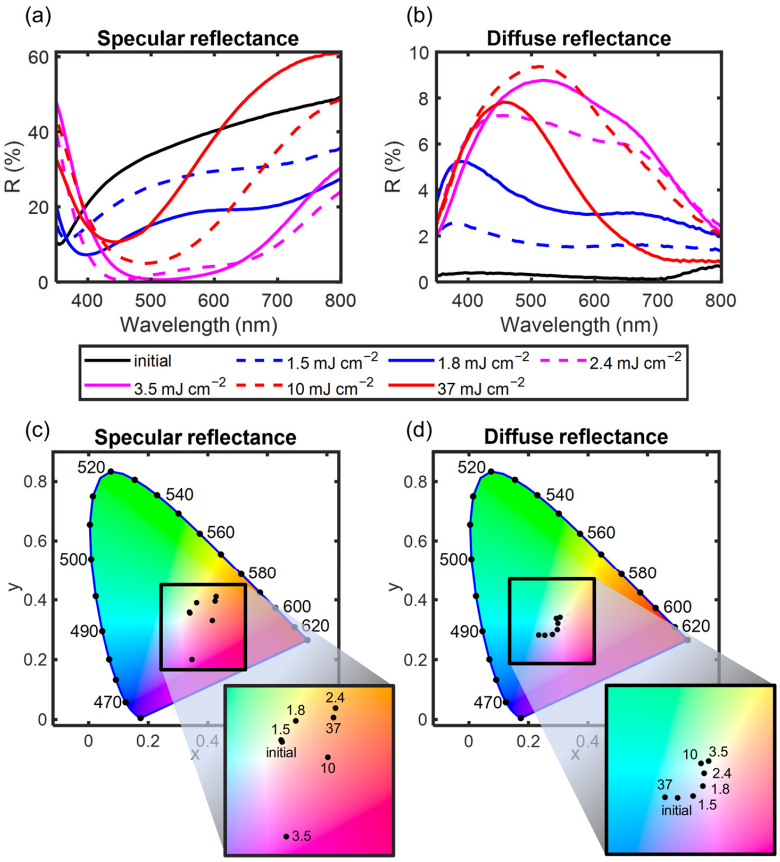

Figure 3. Spectral characteristics of specular (**a**) and diffuse (**b**) reflectance of unmodified (labeled "initial") and modified (scanned 20 times with fluences: 1.8, 2.4, 3.5, 10, and 37 mJ cm^{-2}) regions of the TAFIM sample. The International Commission on Illumination (CIE) 1931 chromaticity diagrams presenting calculated colors using D65 illuminant of (**c**) specular and (**d**) diffuse reflectance.

Modification with low fluence (1.8 mJ cm^{-2}) decreases specular reflectance as the number of scans increases (see Supplementary Material Figure S3); thus, the darkening is visible in the second bottom row of squares in Figure 2a. The corresponding diffuse reflectance increases with the number of scans. Figure 3c,d show the International Commission on Illumination (CIE) 1931 chromaticity diagrams (using CIE standard illuminant D65 [63], which represents average daylight having a correlated color temperature of approximately 6500 K) with color coordinates (see magnified insets for coordinates corresponding to specific fluence). Specular colors are in the red–yellow part of the CIE diagram, and the

diffuse colors are in the blue–white part of the CIE diagram. The colors of unmodified and laser-modified regions of the TAFIM sample are highly reproducible between realizations on the same sample and for samples from different fabrication processes.

The laser scanning alters the morphology of the top aluminum film (see the SEM images in Figure 2 for different fluence and 20 scans, and Figure S3 for fluence of 1.8 mJ cm^{-2} and the different number of scans). With the increase of the laser fluence or the number of scans, the restructuring of the top thin aluminum film of the TAFIM sample became more pronounced. Transformation of the top densely packed Al film into separated nanostructures produces more structures resonating in the visible spectral range, thus increasing the absorption of the sample. This results in the darkening of the TAFIM sample in the bright field mode. A similar effect has previously been reported for Au and Ag-based samples [22,25,27]. At the same time, the modified structures scatter more light than the initial sample; thus, modified regions become clearly visible when observed in the dark field mode, in which the diffuse reflectance signal is detected.

To illustrate the applicability for anti-counterfeiting, laser marking, and plasmonic color printing applications, we printed a sketch of Nicolaus Copernicus and the solar system (open source image [64]) and a logo of the Institute of Optoelectronics, Military University of Technology (Figure 4). Images were captured using the bright field (Figure 4a,c) and the dark field (Figure 4b,d) mode optical microscope using a 2.5× objective lens. The regions were modified with different fluence (from 1.8 to 21 mJ cm^{-2}) using 20 scans. As expected from the data reported above, the images change when the observation mode changes from bright to dark. The modified regions become darker (appear as red/brown) than the initial structure when observed in the bright field mode. When observed in the dark field mode, they "light up" and appear blueish. The negative image effect showing up when changing illumination and observation from bright to dark field mode is a new method that could be used for printing anti-counterfeiting and security features. Qualitatively, the same negative image effect is visible with the naked eye or a generic digital camera (Supplementary Material Figure S5).

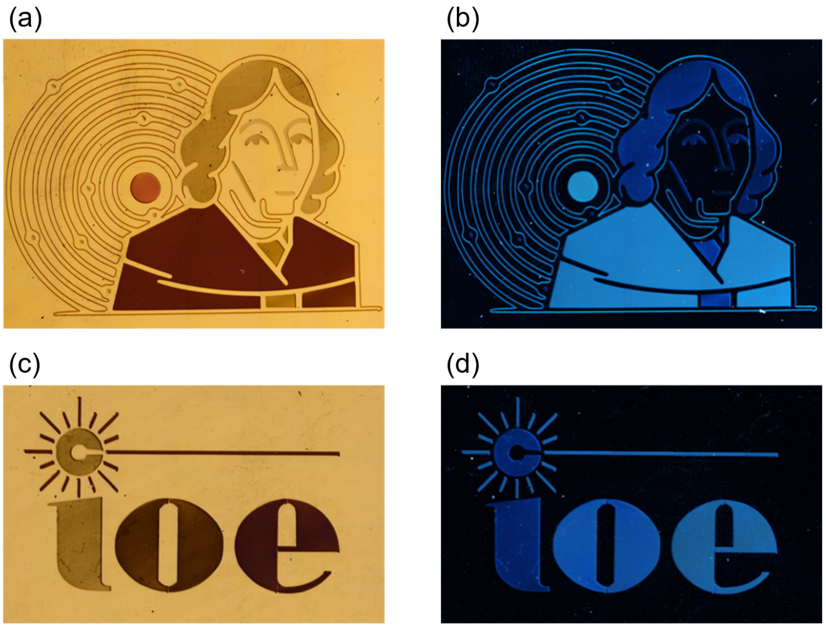

Figure 4. Laser-written images on the TAFIM sample. Images were collected using an optical microscope in (**a**,**c**) bright field and (**b**,**d**) dark field mode. (**a**,**b**) Sketch of Nicolaus Copernicus and the solar system (modified open source image [64]). (**c**,**d**) The logo of the Institute of Optoelectronics of the Military University of Technology. Modified regions were scanned 20 times with fluence in the 1.8–21 mJ cm^{-2} range. The Copernicus image size is 8.7 × 6.6 mm, while the logo image size is 5.9 × 3.7 mm.

The palette of attainable colors could be expanded through changes in the fabrication process, e.g., spacer thickness and refractive index (Figure S1), as it was reported in [25] that the range of attainable colors through laser modification of metal–isolator–metal samples depends on the initial color of the sample. In addition, the sample color could be changed by adding a dielectric layer on top of the modified structure [25].

3.2. Time Stability

To verify the stability of the sample, we measured its specular and diffuse reflectance shortly after deposition and laser modification with a laser fluence of 1.8 and 3.5 mJ cm^{-2} (solid lines in Figure 5), and after 8 (dotted lines in Figure 5), 18 (dashed lines in Figure 5) and 28 (dash-dotted lines in Figure 5) months of storage in the ambient atmosphere at room temperature. Both the unmodified and modified regions show excellent stability for 8 months and good stability for at least 28 months. There is a slight decrease in specular reflectance of the initial region, and an even smaller change is observed for the region modified with 1.8 mJ cm^{-2}. However, no deterioration of the region modified at 3.5 mJ cm^{-2} was observed. The reason for the stability of aluminum nanostructures is their self-passivation [58], and probably, the laser modification of the top thin aluminum film induces additional passivation as compared to the effect observed for the initial structure [65,66]. The observed stability proves the applicability of TAFIM structures for long-lasting plasmonic color-based products.

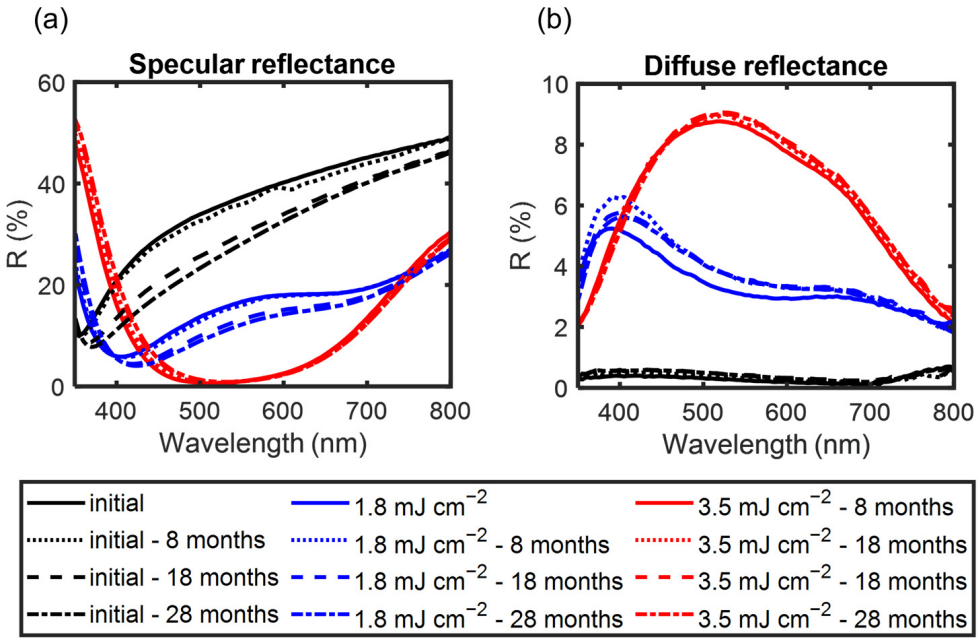

Figure 5. Time stability of the reflectance of the TAFIM sample. Specular (**a**) and diffuse (**b**) reflectances of unmodified (initial) and laser-modified regions of the TAFIM sample were measured shortly after the fabrication (solid lines) and after storing in an ambient atmosphere for 8 (dotted lines), 18 (dashed lines), and 28 (dash-dotted lines) months. The modified regions were scanned 20 times with fluence of 1.8 (blue lines) and 3.5 mJ cm^{-2} (red lines).

4. Conclusions

Our results demonstrate that femtosecond laser modification of semicontinuous aluminum films can be used for rapid plasmonic color printing. Aluminum films are an excellent alternative to silver and gold-based plasmonic random films in plasmonic structural color applications, as the self-passivation of aluminum results in a long-lasting, non-fading coloration effect. Thus, it is crucial that no protective layer for environmental

stability is necessary. Laser-induced structuring of the semicontinuous aluminum film–isolator–metal mirror structure can significantly alter the specular and diffuse reflectance of the sample. The modification fluence threshold is on the order of one mJ cm^{-2}. The "negative image" effect is possible, where a dark field observation mode image is a negative of a bright field observation mode image. Multiplexing of images, for example, hidden images visible in diffuse reflectance observation mode, is possible. The presented technique opens a new cost-effective avenue for color printing and macroscopic and microscopic marking for fine arts, aesthetics, security, and anti-counterfeiting applications. Furthermore, control of the diffuse reflectance component of plasmonic multilayer structures could be beneficial for plasmon-enhanced sensing applications.

Supplementary Materials: The following supporting information can be downloaded at https://www.mdpi.com/article/10.3390/coatings14101298/s1: Figure S1. Simulated reflectance and color of the TAFIM sample for TiO_2 spacer layer ranging from 30 nm to 100 nm; Figure S2. Comparison of experimental and simulated reflectances of the TAFIM sample; Figures S3 and S4. Specular and diffuse reflectance and SEM images of the initial TAFIM sample and after modification with a different number of scans by femtosecond laser with 1.8 mJ cm^{-2} fluence; Figure S5. Optical camera pictures of laser-written images on the TAFIM sample.

Author Contributions: Conceptualization, P.N.; methodology, P.N.; software P.N. and M.P.N.; validation, P.N. and M.P.N.; formal analysis, P.N. and M.P.N.; investigation, M.P.N., B.S., M.P., T.W., B.B., U.C., M.J. and P.N.; resources, P.N. and Y.S.; data curation, M.P.N. and P.N.; writing—original draft preparation, P.N. and M.P.N.; writing—review and editing, P.N., M.P.N. and P.W.; visualization, M.P.N., M.J. and P.N.; supervision, P.N., P.W. and Y.S.; project administration, P.N.; funding acquisition, P.N. All authors have read and agreed to the published version of the manuscript.

Funding: This research was funded by the Military University of Technology under research projects UGB 23-759 and UGB 22-725.

Institutional Review Board Statement: Not applicable.

Informed Consent Statement: Not applicable.

Data Availability Statement: The original contributions presented in the study are included in the article/Supplementary Materials; further inquiries can be directed to the corresponding author.

Acknowledgments: The authors thank Joanna Niedziółka-Jönsson from the Institute of Physical Chemistry, Poland, for access to the optical microscope and Bartłomiej J. Jankiewicz from the Military University of Technology, Poland, for access to the UV-VIS and UV-VIS-IR spectrometers.

Conflicts of Interest: Author Bogusz Stępak and Yuriy Stepanenko were employed by the company Fluence Sp. z o.o. The remaining authors declare that the research was conducted in the absence of any commercial or financial relationships that could be construed as a potential conflict of interest.

References

1. Kinoshita, S.; Yoshioka, S.; Miyazaki, J. Physics of structural colors. *Rep. Prog. Phys.* **2008**, *71*, 076401. [CrossRef]
2. Kinoshita, S.; Yoshioka, S.; Kawagoe, K. Mechanisms of structural colour in the Morpho butterfly: Cooperation of regularity and irregularity in an iridescent scale. *Proc. R. Soc. B Biol. Sci.* **2002**, *269*, 1417–1421. [CrossRef]
3. Schultz, T.D.; Rankin, M.A. Developmental Changes in the Interference Reflectors and Colorations of Tiger Beetles (Cicindela). *J. Exp. Biol.* **1985**, *117*, 111–117. [CrossRef]
4. Cai, W.; Chettiar, U.K.; Yuan, H.-K.; de Silva, V.C.; Kildishev, A.V.; Drachev, V.P.; Shalaev, V.M. Metamagnetics with rainbow colors. *Opt. Express* **2007**, *15*, 3333. [CrossRef]
5. Kumar, K.; Duan, H.; Hegde, R.S.; Koh, S.C.W.; Wei, J.N.; Yang, J.K.W. Printing colour at the optical diffraction limit. *Nat. Nanotechnol.* **2012**, *7*, 557–561. [CrossRef]
6. Song, M.; Feng, L.; Huo, P.; Liu, M.; Huang, C.; Yan, F.; Lu, Y.Q.; Xu, T. Versatile full-colour nanopainting enabled by a pixelated plasmonic metasurface. *Nat. Nanotechnol.* **2023**, *18*, 71–78. [CrossRef]
7. Vynck, K.; Pacanowski, R.; Agreda, A.; Dufay, A.; Granier, X.; Lalanne, P. The visual appearances of disordered optical metasurfaces. *Nat. Mater.* **2022**, *21*, 1035–1041. [CrossRef]
8. Heydari, E.; Sperling, J.R.; Neale, S.L.; Clark, A.W. Plasmonic Color Filters as Dual-State Nanopixels for High-Density Microimage Encoding. *Adv. Funct. Mater.* **2017**, *27*, 1701866. [CrossRef]

9. Tan, S.J.; Zhang, L.; Zhu, D.; Goh, X.M.; Wang, Y.M.; Kumar, K.; Qiu, C.W.; Yang, J.K.W. Plasmonic color palettes for photorealistic printing with aluminum nanostructures. *Nano Lett.* **2014**, *14*, 4023–4029. [CrossRef]
10. Huang, Y.W.; Chen, W.T.; Tsai, W.Y.; Wu, P.C.; Wang, C.M.; Sun, G.; Tsai, D.P. Aluminum plasmonic multicolor meta-Hologram. *Nano Lett.* **2015**, *15*, 3122–3127. [CrossRef]
11. Zhao, J.; Yu, X.; Zhou, K.; Zhang, W.; Yuan, W.; Yu, Y. Polarization-sensitive subtractive structural color used for information encoding and dynamic display. *Opt. Lasers Eng.* **2021**, *138*, 106421. [CrossRef]
12. Ng, R.J.H.; Krishnan, R.V.; Wang, H.; Yang, J.K.W. Darkfield colors from multi-periodic arrays of gap plasmon resonators. *Nanophotonics* **2020**, *9*, 533–545. [CrossRef]
13. Xie, Z.-W.; Yang, J.-H.; Vashistha, V.; Lee, W.; Chen, K.-P. Liquid-crystal tunable color filters based on aluminum metasurfaces. *Opt. Express* **2017**, *25*, 30764. [CrossRef]
14. Zhu, X.; Vannahme, C.; Højlund-Nielsen, E.; Mortensen, N.A.; Kristensen, A. Plasmonic colour laser printing. *Nat. Nanotechnol.* **2016**, *11*, 325–329. [CrossRef] [PubMed]
15. Zhang, Y.; Shi, L.; Hu, D.; Chen, S.; Xie, S.; Lu, Y.; Cao, Y.; Zhu, Z.; Jin, L.; Guan, B.-O.; et al. Full-visible multifunctional aluminium metasurfaces by in situ anisotropic thermoplasmonic laser printing. *Nanoscale Horiz.* **2019**, *4*, 601–609. [CrossRef]
16. Wang, H.; Ruan, Q.; Wang, H.; Rezaei, S.D.; Lim, K.T.P.; Liu, H.; Zhang, W.; Trisno, J.; Chan, J.Y.E.; Yang, J.K.W. Full Color and Grayscale Painting with 3D Printed Low-Index Nanopillars. *Nano Lett.* **2021**, *21*, 4721–4729. [CrossRef]
17. Song, M.; Wang, D.; Kudyshev, Z.A.; Xuan, Y.; Wang, Z.; Boltasseva, A.; Shalaev, V.M.; Kildishev, A.V. Enabling Optical Steganography, Data Storage, and Encryption with Plasmonic Colors. *Laser Photonics Rev.* **2021**, *15*, 2000343. [CrossRef]
18. Lee, H.S.; Shim, T.S.; Hwang, H.; Yang, S.M.; Kim, S.H. Colloidal photonic crystals toward structural color palettes for security materials. *Chem. Mater.* **2013**, *25*, 2684–2690. [CrossRef]
19. Dobrowolski, J.A. Versatile computer program for absorbing optical thin film systems. *Appl. Opt.* **1981**, *20*, 74. [CrossRef]
20. Kats, M.A.; Blanchard, R.; Genevet, P.; Capasso, F. Nanometre optical coatings based on strong interference effects in highly absorbing media. *Nat. Mater.* **2013**, *12*, 20–24. [CrossRef]
21. Roberts, A.S.; Novikov, S.M.; Yang, Y.; Chen, Y.; Boroviks, S.; Beermann, J.; Mortensen, N.A.; Bozhevolnyi, S.I. Laser Writing of Bright Colors on Near-Percolation Plasmonic Reflector Arrays. *ACS Nano* **2019**, *13*, 71–77. [CrossRef] [PubMed]
22. Nyga, P.; Chowdhury, S.N.; Kudyshev, Z.; Thoreson, M.D.; Kildishev, A.V.; Shalaev, V.M.; Boltasseva, A. Laser-induced color printing on semicontinuous silver films: Red, green and blue. *Opt. Mater. Express* **2019**, *9*, 1528. [CrossRef]
23. Nowak, M.P.; Stępak, B.; Pielach, M.; Stepanenko, Y.; Wojciechowski, T.; Bartosewicz, B.; Chodorow, U.; Wachulak, P.; Nyga, P. Femtosecond laser modification of plasmonic color and diffuse reflectance of semicontinuous aluminum film-insulator-metal mirror structures. In *Proceedings SPIE 12131, Nanophotonics IX, 121310W (24 May 2022)*; SPIE: Bellingham, WA, USA, 2022; p. 90. [CrossRef]
24. Cencillo-Abad, P.; Franklin, D.; Mastranzo-Ortega, P.; Sanchez-Mondragon, J.; Chanda, D. Ultralight plasmonic structural color paint. *Sci. Adv.* **2023**, *9*, eadf7207. [CrossRef]
25. Chowdhury, S.N.; Nyga, P.; Kudyshev, Z.A.; Bravo, E.G.; Lagutchev, A.S.; Kildishev, A.V.; Shalaev, V.M.; Boltasseva, A. Lithography-Free Plasmonic Color Printing with Femtosecond Laser on Semicontinuous Silver Films. *ACS Photonics* **2021**, *8*, 521–530. [CrossRef]
26. Nyga, P.; Kildishev, A.V.; Chowdhury, S.N.; Boltasseva, A.; Kudyshev, Z.; Shalaev, V.M. Optical Device, Method of Using the Same, and Method of Making the Same. US11733507B2, 22 August 2023.
27. Chowdhury, S.N.; Simon, J.; Nowak, M.P.; Pagadala, K.; Nyga, P.; Fruhling, C.; Bravo, E.G.; Maćkowski, S.; Shalaev, V.M.; Kildishev, A.V.; et al. Wide-Range Angle-Sensitive Plasmonic Color Printing on Lossy-Resonator Substrates. *Adv. Opt. Mater.* **2023**, *12*, 2301678. [CrossRef]
28. Geng, J.; Xu, L.; Yan, W.; Shi, L.; Qiu, M. High-speed laser writing of structural colors for full-color inkless printing. *Nat. Commun.* **2023**, *14*, 565. [CrossRef]
29. Destouches, N.; Sharma, N.; Vangheluwe, M.; Dalloz, N.; Vocanson, F.; Bugnet, M.; Hébert, M.; Siegel, J. Laser-Empowered Random Metasurfaces for White Light Printed Image Multiplexing. *Adv. Funct. Mater.* **2021**, *31*, 2010430. [CrossRef]
30. Dalloz, N.; Le, V.D.; Hebert, M.; Eles, B.; Figueroa, M.A.F.; Hubert, C.; Ma, H.; Sharma, N.; Vocanson, F.; Ayala, S.; et al. Anti-Counterfeiting White Light Printed Image Multiplexing by Fast Nanosecond Laser Processing. *Adv. Mater.* **2022**, *34*, 2104054. [CrossRef]
31. Kristensen, A.; Yang, J.K.W.; Bozhevolnyi, S.I.; Link, S.; Nordlander, P.; Halas, N.J.; Mortensen, N.A. Plasmonic colour generation. *Nat. Rev. Mater.* **2016**, *2*, 16088. [CrossRef]
32. Song, M.; Wang, D.; Peana, S.; Choudhury, S.; Nyga, P.; Kudyshev, Z.A.; Yu, H.; Boltasseva, A.; Shalaev, V.M.; Kildishev, A.V. Colors with plasmonic nanostructures: A full-spectrum review. *Appl. Phys. Rev.* **2019**, *6*, 041308. [CrossRef]
33. Rezaei, S.D.; Dong, Z.; Chan, J.Y.E.; Trisno, J.; Ng, R.J.H.; Ruan, Q.; Qiu, C.W.; Mortensen, N.A.; Yang, J.K.W. Nanophotonic Structural Colors. *ACS Photonics* **2021**, *8*, 18–33. [CrossRef]
34. Song, M.; Kudyshev, Z.A.; Yu, H.; Boltasseva, A.; Shalaev, V.M.; Kildishev, A.V. Achieving full-color generation with polarization-tunable perfect light absorption. *Opt. Mater. Express* **2019**, *9*, 779. [CrossRef]
35. Feng, R.; Wang, H.; Cao, Y.; Zhang, Y.; Ng, R.J.H.; Tan, Y.S.; Sun, F.; Qiu, C.W.; Yang, J.K.W.; Ding, W. A Modular Design of Continuously Tunable Full Color Plasmonic Pixels with Broken Rotational Symmetry. *Adv. Funct. Mater.* **2022**, *32*, 2108437. [CrossRef]

36. Wang, H.C.; Martin, O.J.F. Polarization-Controlled Chromo-Encryption. *Adv. Opt. Mater.* **2023**, *11*, 2202165. [CrossRef]
37. Bao, Y.; Yu, Y.; Xu, H.; Lin, Q.; Wang, Y.; Li, J.; Zhou, Z.K.; Wang, X.H. Coherent Pixel Design of Metasurfaces for Multidimensional Optical Control of Multiple Printing-Image Switching and Encoding. *Adv. Funct. Mater.* **2018**, *28*, 1805306. [CrossRef]
38. Zijlstra, P.; Chon, J.W.M.; Gu, M. Five-dimensional optical recording mediated by surface plasmons in gold nanorods. *Nature* **2009**, *459*, 410–413. [CrossRef]
39. Novikov, S.M.; Frydendahl, C.; Beermann, J.; Zenin, V.A.; Stenger, N.; Coello, V.; Mortensen, N.A.; Bozhevolnyi, S.I. White Light Generation and Anisotropic Damage in Gold Films near Percolation Threshold. *ACS Photonics* **2017**, *4*, 1207–1215. [CrossRef]
40. Rezaei, S.D.; Dong, Z.; Wang, H.; Xu, J.; Wang, H.; Yaraki, M.T.; Goh, K.C.H.; Zhang, W.; Ghorbani, S.R.; Liu, X.; et al. Tri-functional metasurface enhanced with a physically unclonable function. *Mater. Today* **2023**, *62*, 51–61. [CrossRef]
41. Liu, H.; Xu, J.; Wang, H.; Liu, Y.; Ruan, Q.; Wu, Y.; Liu, X.; Yang, J.K.W. Tunable Resonator-Upconverted Emission (TRUE) Color Printing and Applications in Optical Security. *Adv. Mater.* **2019**, *31*, 1807900. [CrossRef]
42. Yagil, Y.; Gadenne, P.; Julien, C.; Deutscher, G. Optical properties of thin semicontinuous gold films over a wavelength range of 2.5 to 500 μm. *Phys. Rev. B* **1992**, *46*, 2503–2511. [CrossRef]
43. Nyga, P.; Drachev, V.P.; Thoreson, M.D.; Shalaev, V.M. Mid-IR plasmonics and photomodification with Ag films. *Appl. Phys. B* **2008**, *93*, 59–68. [CrossRef]
44. Chettiar, U.K.; Nyga, P.; Thoreson, M.D.; Kildishev, A.V.; Drachev, V.P.; Shalaev, V.M. FDTD modeling of realistic semicontinuous metal films. *Appl. Phys. B* **2010**, *100*, 159–168. [CrossRef]
45. Ooms, M.D.; Jeyaram, Y.; Sinton, D. Disposable Plasmonics: Rapid and Inexpensive Large Area Patterning of Plasmonic Structures with CO2 Laser Annealing. *Langmuir* **2015**, *31*, 5252–5258. [CrossRef] [PubMed]
46. Janicki, V.; Amotchkina, T.V.; Sancho-Parramon, J.; Zorc, H.; Trubetskov, M.K.; Tikhonravov, A.V. Design and production of bicolour reflecting coatings with Au metal island films. *Opt. Express* **2011**, *19*, 25521. [CrossRef]
47. Shalaev, V.M. Electromagnetic properties of small-particle composites. *Phys. Rep.* **1996**, *272*, 61–137. [CrossRef]
48. Genov, D.A.; Sarychev, A.K.; Shalaev, V.M. Metal-dielectric composite filters with controlled spectral windows of transparency. *J. Nonlinear Opt. Phys. Mater.* **2003**, *12*, 419–440. [CrossRef]
49. Søndergaard, T.; Bozhevolnyi, S. Slow-plasmon resonant nanostructures: Scattering and field enhancements. *Phys. Rev. B-Condens. Matter Mater. Phys.* **2007**, *75*, 073402. [CrossRef]
50. Sarychev, A.K.; Barbillon, G.; Ivanov, A. Nanogap Plasmon Resonator: An Analytical Model. *Appl. Sci.* **2023**, *13*, 12882. [CrossRef]
51. Zhu, X.; Engelberg, J.; Remennik, S.; Zhou, B.; Pedersen, J.N.; Jepsen, P.U.; Levy, U.; Kristensen, A. Resonant Laser Printing of Optical Metasurfaces. *Nano Lett.* **2022**, *22*, 2786–2792. [CrossRef]
52. Seo, M.; Kim, J.; Oh, H.; Kim, M.; Baek, I.U.; Choi, K.D.; Byun, J.Y.; Lee, M. Printing of Highly Vivid Structural Colors on Metal Substrates with a Metal-Dielectric Double Layer. *Adv. Opt. Mater.* **2019**, *7*, 1900196. [CrossRef]
53. Vorobyev, A.Y.; Guo, C. Enhanced absorptance of gold following multipulse femtosecond laser ablation. *Phys. Rev. B* **2005**, *72*, 195422. [CrossRef]
54. Guay, J.-M.; Lesina, A.C.; Côté, G.; Charron, M.; Poitras, D.; Ramunno, L.; Berini, P.; Weck, A. Laser-induced plasmonic colours on metals. *Nat. Commun.* **2017**, *8*, 16095. [CrossRef]
55. West, P.R.; Ishii, S.; Naik, G.V.; Emani, N.K.; Shalaev, V.M.; Boltasseva, A. Searching for better plasmonic materials. *Laser Photonics Rev.* **2010**, *4*, 795–808. [CrossRef]
56. Yokogawa, S.; Burgos, S.P.; Atwater, H.A. Plasmonic color filters for CMOS image sensor applications. *Nano Lett.* **2012**, *12*, 4349–4354. [CrossRef]
57. Ayas, S.; Topal, A.E.; Cupallari, A.; Güner, H.; Bakan, G.; Dana, A. Exploiting Native Al_2O_3 for Multispectral Aluminum Plasmonics. *ACS Photonics* **2014**, *1*, 1313–1321. [CrossRef]
58. Knight, M.W.; King, N.S.; Liu, L.; Everitt, H.O.; Nordlander, P.; Halas, N.J. Aluminum for plasmonics. *ACS Nano* **2014**, *8*, 834–840. [CrossRef]
59. Olson, J.; Manjavacas, A.; Liu, L.; Chang, W.S.; Foerster, B.; King, N.S.; Knight, M.W.; Nordlander, P.; Halas, N.J.; Link, S. Vivid, full-color aluminum plasmonic pixels. *Proc. Natl. Acad. Sci. USA* **2014**, *111*, 14348–14353. [CrossRef] [PubMed]
60. Shrestha, V.R.; Lee, S.-S.; Kim, E.-S.; Choi, D.-Y. Aluminum Plasmonics Based Highly Transmissive Polarization-Independent Subtractive Color Filters Exploiting a Nanopatch Array. *Nano Lett.* **2014**, *14*, 6672–6678. [CrossRef]
61. Pascoe, K. Reflectivity and Transmissivity through Layered, Lossy Media: A User-Friendly Approach. 2001. Available online: https://community.ptc.com/sejnu66972/attachments/sejnu66972/PTCMathcad/85134/1/ADA389099%20Reflectivity%20and%20Transmissivity%20through%20Layered,%20Lossy%20Media=%20A%20User-Friendly%20Approach.pdf (accessed on 14 September 2020).
62. Ohta, N.; Robertson, A.R. *Colorimetry: Fundamentals and Applications*; John Wiley & Sons: Hoboken, NJ, USA, 2006. Available online: https://books.google.com/books/about/Colorimetry.html?id=U8jeh1uhSHgC (accessed on 31 March 2023).
63. *CIE 2022*; CIE Standard Illuminant D65. International Commission on Illumination (CIE): Vienna, Austria, 2022. [CrossRef]
64. Available online: https://www.pngegg.com/pl/png-dbtme (accessed on 14 May 2021).

65. Okoshi, M.; Iwai, K.; Nojiri, H.; Inoue, N. F2-laser-induced modification of aluminum thin films into transparent aluminum oxide. *Jpn. J. Appl. Phys.* **2012**, *51*, 122701. [CrossRef]
66. Fan, P.; Sun, Z.; Wilkes, G.C.; Gupta, M.C. Low-temperature laser generated ultrathin aluminum oxide layers for effective c-Si surface passivation. *Appl. Surf. Sci.* **2019**, *480*, 35–42. [CrossRef]